Choriocapillaris impairment around the atrophic lesions in patients with geographic atrophy: a swept-source optical coherence tomography angiography study.

Marco Nassisi[1,2], Yue Shi[1,2], Wenying Fan[1,2,3], Enrico Borrelli[1,2,4], Akihito Uji[1,2], Michael Ip[1,2], Srinivas R. Sadda[1,2].

1. Doheny Image Reading Center, Doheny Eye Institute, 1350 San Pablo St., DVRC211, Los Angeles, CA, 90033, USA.

2. Department of Ophthalmology, David Geffen School of Medicine at UCLA, Los Angeles, CA, USA.

3. Beijing Tongren Eye Center, Beijing Tongren Hospital, Beijing Ophthalmology and Visual Sciences Key, Laboratory, Capital Medical University, Beijing, China.

4. Ophthalmology Clinic, Department of Medicine and Science of Ageing, University G. D'Annunzio Chieti-Pescara, Chieti, Italy.

Corresponding Author:

SriniVas R. Sadda, MD

1355 San Pablo Street, Suite 211,

Los Angeles California 90033, United States

Tel: 323-342-6503 Fax: 323-442-6460

E-mail: SSadda@doheny.org

Number of words: 3351

Precis

Using swept-source optical coherence tomography angiography in eyes with geographic atrophy, a significant impairment in choriocapillaris flow was found around the atrophic lesions. Choriocapillaris alterations may be relevant to the progression of geographic atrophy.

Abstract

Aims: To evaluate the choriocapillaris (CC) flow alterations around geographic atrophy (GA) in eyes with dry age-related macular degeneration (AMD).

Methods: Using a swept-source optical-coherence tomography angiography (SS-OCTA) device, two volume 6 x 6 mm scans were acquired in patients with GA presenting between June and December 2017 at the Doheny - UCLA Eye Centers. The area of GA was delineated on the *en face* structural OCT fundus images. For each eye, the *en-face* OCTA slabs at the level of the CC from the two acquisitions were averaged and compensated for signal loss using the corresponding structural *en-face* images. The resulting images were binarized and analyzed for the percentage of flow voids in the *para-atrophy zone* (a 500 μm wide ring around the immediate edge of the atrophy) and in the *peri-atrophy zone* (a 500 μm wide ring around the *para-atrophy zone* edge), the latter considered as a reference in the comparative analysis.

Results: Thirty eyes of 20 patients were enrolled. The percentage of flow voids in the *para-atrophy zone* was 27.23 ± 6.29 %, and was significantly higher than in the surrounding *peri-atrophy zone* (23.4 ± 6.01 % ;p- value < 0.001). There was no significant correlation between the flow void percentage in these regions and age, visual acuity, extent of the atrophic area, or central choroidal thickness.

Conclusions: A significant impairment of the CC flow is present in the zone immediately surrounding the GA lesions strengthening the hypothesis that CC alterations may be relevant to the progression of GA.

Introduction

Geographic atrophy (GA) is a late stage manifestation of dry age-related macular degeneration (AMD). It is defined as any sharply delineated roughly round or oval area of hypopigmentation or depigmentation with increased visibility of the underlying choroidal vessels and of at least 175 μm in diameter on 30 or 35 degrees color fundus images[1].

A more recent optical coherence tomography (OCT) based classification defines GA as complete retinal pigment epithelium (RPE) and outer retinal atrophy (cRORA), in the absence of choroidal neovascularization (CNV) (present or previous), measuring at least 250 microns in diameter[2].

GA results from the degeneration of photoreceptors, retinal pigment epithelium (RPE), and choriocapillaris (CC). Nevertheless, while the RPE and outer retinal degeneration are well visualized using OCT, CC disruption is difficult to identify *in vivo* on structural OCT alone. OCT angiography (OCTA) is a recent technique that allows the visualization of the retinal vascular networks in a depth-resolved fashion,[3] making it possible to visualize the loss of CC flow under the atrophic patches[4] in patients with GA. Recently *Sacconi et al.*, using a spectral domain (SD)-OCTA device, demonstrated that the CC flow impairment can be observed in areas around the atrophic lesions even where the RPE appears to be intact[5].

Whether the RPE or the CC disruption occurs first is still a topic of debate,[6–11] and the relatively poor depth penetration of the SD-OCTA may compromise CC assessment, particularly in the presence of overlying deposits or retinal thickening with an intact RPE. Indeed, the 840 nm light wavelength utilized by most SD-OCT devices is highly scattered by the RPE, limiting light penetration into the choroid[12–14].

Swept-source OCTA (SS-OCTA) uses a different light to obtain the en-face images of the vascular networks. Using a longer wavelength (1050 nm), the SS-OCTA offers a deeper light penetration and provides higher quality images of the CC meshwork which may resemble histologic images in heathy eyes[15]. Furthermore the quality of the images may be significantly improved with post-acquisition processing methods such as the averaging of multiple images from multiple acquisitions[16,17].

In pathologic eyes, disease features and lesions may further impact the visualization of the CC. For example, thick drusenoid deposits can attenuate or scatter the incident light creating a "shadowing" effect on the underlying CC. Although this shadowing effect is less pronounced compared with SD-OCT,

these alterations may confound quantitative analysis of the underlying CC. Recently *Zhang et al.* developed a simple strategy to compensate this signal loss under drusen combining the *en-face* structural images with the respective angiograms[18].

In this study we used a combination of averaging and signal compensation on images acquired with a SS-OCTA, in order to better study the CC flow around the areas of geographic atrophy, where the RPE appears to still be preserved.

Methods

In this prospective study, we acquired SS-OCTA images of consecutive patients with GA who were evaluated at the Doheny-UCLA Eye Centers by one physician (SRS) between June and December 2017. Eligible patients had GA in at least one eye without evidence of any other pathology involving the macula. Eyes with non-visually significant vitreoretinal interface disease, such as a subtle epiretinal membrane only visible by OCT, were not excluded. Myopia greater than 6 diopters and presence of significant media opacities which could impact the quality of the OCT images were exclusion criteria for this study.

The study was performed in accordance with the Health Insurance Portability and Accountability Act and adhered to the principles of the Declaration of Helsinki. All patients signed a written informant consent to participate in this observational study. The informed consent and research was approved by the institutional review board (IRB) of the University of California – Los Angeles (UCLA).

All patients underwent a complete ophthalmic examination, including best-corrected visual acuity (BCVA) using Early Treatment Diabetic Retinopathy Study (ETDRS) charts, slit lamp biomicroscopy, tonometry and SS-OCTA.

Central choroidal thickness (CCT) was assessed by manually measuring at foveal center from Bruch's membrane to the sclera-choroidal border. To ensure the repeatability of the method, the measurements were repeated twice by two independent operators.

Imaging

Patients underwent SS-OCTA imaging with the PLEX Elite 9000 device (Carl Zeiss Meditec Inc., Dublin, CA, USA) which uses a swept laser source with a central wavelength of 1050 nm (1000–1100 nm full bandwidth) and operates at 100,000 A-scans per second. This instrument employs a full-width at half-maximum (FWHM) axial resolution of approximately 5 μm in tissue, and a lateral resolution at the retinal surface estimated at approximately 14 μm. OCTA imaging of the macula was performed using a scan pattern with a 6 X 6 mm area (500 A-scans x 500 B-scans) centered on the fovea. Each eye was repeatedly imaged with pupil dilation to obtain two OCTA volume scan sets with sufficient image quality (signal strength index (SSI)>7) that fulfilled the acceptance criteria of the Doheny Image Reading Center (DIRC), as previously reported.[17,19]

A fully-automated retinal layer segmentation algorithm was applied to the three-dimensional structural OCT data, in order to segment the CC slab as defined previously (10 μm thick starting 31 μm below the RPE reference).[20] This segmentation was then applied to OCTA flow intensity data to obtain vascular images. Maximum projection analyses of the flow intensity were performed to generate the *en-face* images of the CC plexus (1024x1024 pixels). Before exporting all angiograms, projection artifact removal was performed using the automated algorithm of the instrument software[21,22].

Post-acquisition image processing

To compensate for CC signal attenuation resulting from the RPE and pathologic alterations at RPE/BM complex level (e.g. basal laminar deposits) , a previously described method was applied [18]. Briefly, for each eye, the CC layer was first segmented from the structural OCT and the associated flow slab was then identified from the angiogram. An inverse transformation was applied to the *en-face* structural CC image to enhance the attenuated signal under drusen, where a Gaussian smoothing filter (3 X 3 pixel kernel) was used to minimize speckle noise. Then, a multiplication between the *en-face* CC flow image and the smoothed, inverted CC structural image was performed. By this approach, the shadowing effect under drusenoid depoists was compensated while the signal in unaffected regions remained unchanged (Figure 1).

For each eye, the resulting compensated CC *en-face* images generated from 2 different OCTA cube scan sets were stacked to create a 2-frame video and were registered before multiple image averaging. A central square area of 819x819 pixels was cropped for registration and averaging. Registration was first performed on the 2-frame video based on the superficial capillary plexus *en-face* images, as previously reported.[17] This same transformation was then applied to the CC layer, as described in detail in a previous publication.[23] After registration, the 2 frames of the CC were compounded into a single image by projecting the average intensity (Figure 1).

Quantitative image analysis

The resultant averaged CC *en-face* image was exported and analyzed using ImageJ software version 1.50 (National Institutes of Health, Bethesda, MD; available at http://rsb.info.nih.gov/ij/index.html)[24] and binarized for quantitative image analysis of the signal voids. The Phansalkar method (radius, 15 pixels) was used to binarize the images, as previously

described.[20,23,25] These images were then processed with the 'Analyze Particles' command, in order to count the flow voids as a percentage of the area analyzed.

The quantitative analysis was performed over two concentric 500-μm-wide rings around the GA lesion edge (following the contour of the GA lesion) to assess the CC surrounding the atrophy (Figure 2).

The 500 μm cut-off was arbitrarily chosen, in accordance with a previous published study [5]. The inner ring was defined as the *para-atrophy zone*, while the outer ring was defined as the *peri-atrophy zone*. The *peri-atrophy zone* was used as a reference to assess the para-atrophic CC.

To isolate the GA region we used the OCT fundus image as previously described[26]. This image is the *en face* reconstruction of the sum of all the signals coming from each of the A-scans acquired[27]. GA appears as a bright area on the image due to the increased penetration of light into the choroid caused by the overlying RPE and outer retina atrophy[27,28]. The borders of the GA region were manually segmented and verified using the corresponding structural B-scans to ensure the integrity of the RPE outside the selection.

To obtain the *para-atrophy zone*, we used the "Distance Map" ImageJ function on the selected GA region. The "Distance Map" function automatically delineates a border 500 μm displaced from the atrophy edge, exactly following the contour of the GA border. Furthermore, in case of multifocal lesions the "Distance Map" function on the "binarized" image allows us to delimit those areas within 500 μm of the edge of all the atrophy lesions in the image (without any size limit), by excluding areas occupied by adjacent lesions . The *peri-atrophy zone* was determined by applying the same method; specifically, the "distance map" function was used to delineate a border displaced 500 microns from the *para-atrophy zone* edge.

As CC flow voids are believed to show a regional dependence (even in normal eyes) with greater flow voids centrally compared with more peripheral regions of the macula, we performed an additional

8

layer of analysis to exclude this potential confounder. Specifically, for each case, we also selected and

analyzed two 500x500 µm square regions in the *para-* and *peri-atrophy* zones which were equidistant

from the foveal center. The first square was drawn in the *peri-atrophy* zone at the innermost point of its

inner boundary. The second square had to satisfy the following conditions: (1) location in the *para-*

atrophy zone; (2) the difference between the distances of the centers of mass of the two squares from

the fovea should not be more than 10 pixels (Figure 3). If these conditions were not satisfied, the

subject was excluded from this additional analysis. If more than one square could satisfy these

conditions, the closest in distance to the first square was chosen for the analysis.

The entire procedure was repeated by two experienced reading center OCT graders (MN and

WF) in order to investigate the repeatability of all measurements. All values were then averaged for use

in the subsequent statistical analysis.

Statistics

Statistical analyses were performed using SPSS Statistics version 20 (IBM, Armonk, NY).

Intraclass correlation coefficients (ICC) were calculated for atrophy area, CCT and flow voids

measurements. A Wilcoxon signed ranked test was performed to test the difference in percentage of

flow voids in the *para-atrophy zone* versus the *peri-atrophy zone*. Generalized estimating equations

(GEE) were used to compare the means and test the associations between percentage of flow voids and

age, BCVA, CCT and atrophy dimension.

Results

Thirty eyes of 20 patients (6 males, mean age: 85.19 ± 9.25 years) were enrolled in the study. The fellow eyes of 10 patients were excluded for intermediate AMD in 3 eyes, CNV in 5 eyes and the inability to acquire scans of sufficient quality scans in 2 eyes (due to poor fixation).

Mean BCVA was 0.51 ± 0.31 logarithm of the minimum angle of resolution (LogMAR) (median: 0.5 logMAR; range 0 – 1) and the mean CCT was 221.16 ± 161.22 μm (median: 193.5 μm; range: 48 – 767).

The mean area of the GA lesion was 7.86 ± 6.06 mm^2 (median 6.32 mm^2; range: 0.63 - 21.33 mm^2).

The percentage of flow voids in the entire *para-atrophy zone* was 27.23 ± 6.29 % and significantly greater than the surrounding entire *peri-atrophy zone,* where it was 23.4 ± 6.01 % (p value = 0.008).

The additional, comparative analysis of the equidistant 500x500μm *para-atrophy* and *peri-atrophy* squares could be performed in all 30 eyes. The result of this analysis also demonstrated that a significantly higher percentage of flow voids in the *para-atrophy zone* (29.6±7.88 %) compared to the *peri-atrophy zone* (22.8±5.86 %) with a p value <0.001.

GEE analysis found no significant correlations were found between the percentage of flow voids in each zone and various other parameters including age, BCVA, extent of the atrophic area, and CCT.

Repeatability assessment

GA area measurements obtained from manual delineation of the atrophy lesion between graders had an ICC of 0.997 (95% confidence interval (CI) 0.95-0.99). CCT measurements had an ICC of 0.939 (95% CI 0.869-0.972). The calculation of the flow voids percentage in the *peri-atrophy* and *para-*

atrophy zone had an ICC of 0.912 (95% CI 0.895-0.927) for the entire zones and 0.897 (95% CI 0.875-0.923) for the 500x500 μm squares.

Discussion

In this study we investigated the CC around the GA using SS-OCTA and with compensation analysis to mitigate the impact of signal attenuation caused by disease-related alterations at the level of the outer retina/RPE/BM complex. The image of the CC provided by current OCTA instruments shows a granular appearance with small bright regions interspersed with small dark regions. The known anatomic structure of the choriocapillaris does not appear to explain these dark areas, hence they are probably the result of a relative decreases in local flow signal below the threshold of detection. As such, these small areas are called flow voids[20,21]. The analysis of these presumed CC flow voids has been evaluated in many posterior segment diseases and has been inferred to reflect CC impairment relevant to disease pathophysiology[19,25,29–33].

Our findings of a greater extent of flow voids in the CC immediately surrounding the GA lesion compared with more remote regions would appear to support the hypothesis that CC loss may precede overt RPE degeneration since the CC appears to be significantly impaired even in regions where the RPE layer appears to be intact structurally.

Our OCTA findings are consistent with previous histologic studies. *Biesemeier et al.* examined four post-mortem GA eyes using a combination of light and electron microscopy and observed that CC loss occurred in regions underlying intact retina and RPE, and concluded that CC breakdown precedes RPE degeneration in AMD.

Whereas histologic studies provide a direct visualization of the vascular structure, OCTA findings provide insight into CC blood flow; with the absence of OCTA signal indicating the absence of blood flow above the threshold of detection rather than a complete absence of blood flow.[6]

Kvanta et al. reported that CC flow was reduced outside GA lesions extending beyond the GA margin in a qualitative evaluation of CC using SD-OCTA[11]. As previously mentioned, the current commercially available SD-OCT machines using a ~840 nm wavelength may be confounded by signal loss which can impact assessment of the CC in the setting of pathology such as drusen. Furthermore, SD-OCT systems are affected by a signal roll-off that further degrades the signal with depth. Longer wavelength SS-OCT systems are less affected by RPE attenuation and do not suffer from as steep a signal roll-off, making long wavelength SS-OCT ideal for CC imaging.

Recently *Moult et al.* performed a qualitative analysis of the CC in eyes with nascent geographic atrophy and drusen-associated geographic atrophy using SS-OCTA, and demonstrated CC flow impairment not only under the area of the lesions, but also throughout the imaged field[7].

Our study is the first, however, to report quantitative data on the CC around GA using a SS-OCTA approach with further enhancement of image quality using a combination of averaging and signal loss compensation. In particular we focused our analysis on the *para-atrophy* region in order to test our hypothesis that a higher level of impairment would be present in the immediate vicinity of the lesion border where the RPE was still structurally intact. It should be noted, however, that a structurally intact RPE on OCT does not mean a normally functioning RPE.

Sacconi et al. attempted to further clarify this point by comparing the CC flow under the regions surrounding the GA which were rated as hyperautofluorescent on fundus autofluorescence (FAF) images, and compared them to isoautofluorescent regions. While CC flow impairment was present in both regions, it was significantly greater in the hyperautofluorescent areas which are thought be regions

of significant RPE impairment. Based on these findings they hypothesized that the first injury in GA occurs at the level of the CC.

Despite this finding, we would argue that it is still difficult to exclude the possibility that a combination of both RPE and CC flow impairment are relevant to the initiation of the atrophic process. For example, the earliest dysfunction of the RPE may still be undetectable using traditional FAF. Thus, it is still possible that RPE dysfunction could be the primary step in GA development and progression with secondary alterations to the underlying CC (e.g. due to loss of VEGF production by a dysfunctional RPE), leading ultimately to RPE loss and further progression of GA. [8,10].

Given the important purported role of the CC in the development of GA, this uncertainty hinders our understanding of disease pathophysiology and progression. The development of new tools to probe RPE function and health (e.g. fluorescence lifetime imaging ophthalmoscopy) and prospective longitudinal studies investigating the correlation between CC flow impairment and GA progression, may provide additional insights into this question.

Flow voids in CC are thought to demonstrate a regional dependence even in normal eyes, with a higher number of flow voids in central portions of the macula compared to more peripheral regions (personal communication, Phil Rosenfeld). This phenomenon is even more remarkable in older subjects (> 50 years old). Thus, studies comparing CC flow voids within regions of interest in the macula[5], may be confounded by this normal topographical variation in the density of flow voids. To address this potential , we performed an additional analysis comparing the CC within our regions of interest (*para-atrophic* and *peri-atrophic* zones) which were equidistant from the foveal center. We were able to identify such equidistant regions because of irregular and multifocal configurations of our GA lesions. This additional analysis confirmed the apparent higher impairment of CC flow in the region immediately surrounding the GA lesion.

Our study is not without limitations including its cross-sectional nature and small sample size. In addition, as were not able to perform variable inter-scan time analysis (VISTA) we could not distinguish among various levels of severity of CC impairment. Even if such an analysis was employed, however, we would still be limited by the range of flows detectable by current OCTA technology. Also, In our cohort, we included all subjects with GA and did not exclude cases with a pachychoroid GA phenotype[34]. In a post-hoc review, we could identify 3 subjects (3 eyes) who met criteria for pachychoroid GA, but this small number was insufficient to allow a subanalysis of this cohort. We do not believe, however, that these few pachychoroid GA cases influences the main study finding, and the absence of a correlation between the flow voids and the CCT in this cohort would appear to support this contention. Finally, we used only OCT to detect and outline the borders of the GA lesion. While we now have consensus definitions for OCT on atrophy[2], and measurement of atrophy by OCT are well-correlated with measurements from FAF[35,36], FAF and OCT may not be measuring the exact same thing. Even though FAF has been considered the gold standard to identify the areas of atrophy, *en-face* OCT has been shown to be a valuable tool for detecting the lesions (even for earlier lesions such as nascent GA)[26,37,38] and for following their progression[39].

Our study also has many strengths including its prospective design and the use of SS-OCTA. In addition, we used a signal compensation method as well as image averaging to further enhance image quality and reduce the potentially confounding impact of signal attenuation on OCTA-derived CC measurements. Moreover, we developed a method to cope with the irregular border and multifocal nature of GA lesions to more precisely study the status of the surrounding CC. Finally, we addressed the potential confounding effect of regional variations in CC flow voids by comparing regions equidistant from the foveal center.

In summary, our study confirms that significant flow impairment of the CC may be present in regions surrounding GA lesions, further highlighting the relevance of the CC to the pathophysiology of GA. Future larger longitudinal studies will be required in order to determine whether the severity of these surrounding regions of CC flow impairment are predictive of GA progression.

Conflicts of Interest

Funding Statement

Contributorship Statement

Marco Nassisi, Michael Ip and SriniVas R Sadda were involved in study design, collection and analysis of the data as well as drafting of the manuscript. Yue Shi, Wenying Fan, Enrico Borrelli, and Akihito Uji were involved in study design, data collection, and critical review of the manuscript.

References

1. Bird AC, Bressler NM, Bressler SB, et al. An international classification and grading system for age-related maculopathy and age-related macular degeneration. The International ARM Epidemiological Study Group. *Surv Ophthalmol*. 1995;39(5):367-374.

2. Sadda SR, Guymer R, Holz FG, et al. Consensus Definition for Atrophy Associated with Age-Related Macular Degeneration on OCT: Classification of Atrophy Report 3. *Ophthalmology*. November 2017. doi:10.1016/j.ophtha.2017.09.028

3. Gao SS, Jia Y, Zhang M, et al. Optical Coherence Tomography Angiography. *Invest Ophthalmol Vis Sci*. 2016;57(9):OCT27-36. doi:10.1167/iovs.15-19043

4. Waheed NK, Moult EM, Fujimoto JG, Rosenfeld PJ. Optical Coherence Tomography Angiography of Dry Age-Related Macular Degeneration. *Dev Ophthalmol*. 2016;56:91-100. doi:10.1159/000442784

5. Sacconi R, Corbelli E, Carnevali A, Querques L, Bandello F, Querques G. OPTICAL COHERENCE TOMOGRAPHY ANGIOGRAPHY IN GEOGRAPHIC ATROPHY. *Retina Phila Pa*. October 2017. doi:10.1097/IAE.0000000000001873

6. Choi W, Moult EM, Waheed NK, et al. Ultrahigh-Speed, Swept-Source Optical Coherence Tomography Angiography in Nonexudative Age-Related Macular Degeneration with Geographic Atrophy. *Ophthalmology*. 2015;122(12):2532-2544. doi:10.1016/j.ophtha.2015.08.029

7. Moult EM, Waheed NK, Novais EA, et al. SWEPT-SOURCE OPTICAL COHERENCE TOMOGRAPHY ANGIOGRAPHY REVEALS CHORIOCAPILLARIS ALTERATIONS IN EYES WITH NASCENT GEOGRAPHIC ATROPHY AND DRUSEN-ASSOCIATED GEOGRAPHIC ATROPHY. *Retina Phila Pa*. 2016;36 Suppl 1:S2-S11. doi:10.1097/IAE.0000000000001287

8. Mullins RF, Johnson MN, Faidley EA, Skeie JM, Huang J. Choriocapillaris vascular dropout related to density of drusen in human eyes with early age-related macular degeneration. *Invest Ophthalmol Vis Sci*. 2011;52(3):1606-1612. doi:10.1167/iovs.10-6476

9. Biesemeier A, Taubitz T, Julien S, Yoeruek E, Schraermeyer U. Choriocapillaris breakdown precedes retinal degeneration in age-related macular degeneration. *Neurobiol Aging*. 2014;35(11):2562-2573. doi:10.1016/j.neurobiolaging.2014.05.003

10. Schlingemann RO. Role of growth factors and the wound healing response in age-related macular degeneration. *Graefes Arch Clin Exp Ophthalmol Albrecht Von Graefes Arch Klin Exp Ophthalmol*. 2004;242(1):91-101. doi:10.1007/s00417-003-0828-0

11. Kvanta A, Casselholm de Salles M, Amrén U, Bartuma H. OPTICAL COHERENCE TOMOGRAPHY ANGIOGRAPHY OF THE FOVEAL MICROVASCULATURE IN GEOGRAPHIC ATROPHY. *Retina Phila Pa*. 2017;37(5):936-942. doi:10.1097/IAE.0000000000001248

12. Al-Sheikh M, Falavarjani KG, Tepelus TC, Sadda SR. Quantitative Comparison of Swept-Source and Spectral-Domain OCT Angiography in Healthy Eyes. *Ophthalmic Surg Lasers Imaging Retina*. 2017;48(5):385-391. doi:10.3928/23258160-20170428-04

13. Zhang Q, Chen C-L, Chu Z, et al. Automated Quantitation of Choroidal Neovascularization: A Comparison Study Between Spectral-Domain and Swept-Source OCT Angiograms. *Invest Ophthalmol Vis Sci*. 2017;58(3):1506-1513. doi:10.1167/iovs.16-20977

14. Copete S, Flores-Moreno I, Montero JA, Duker JS, Ruiz-Moreno JM. Direct comparison of spectral-domain and swept-source OCT in the measurement of choroidal thickness in normal eyes. *Br J Ophthalmol*. 2014;98(3):334-338. doi:10.1136/bjophthalmol-2013-303904

15. Gorczynska I, Migacz JV, Jonnal R, Zawadzki RJ, Poddar R, Werner JS. Imaging of the human choroid with a 1.7 MHz A-scan rate FDML swept source OCT system. In: *Opthalmic Technologies XXVII*. SPIE; 2017. doi:10.1117/12.2251704

16. Uji A, Balasubramanian S, Lei J, Baghdasaryan E, Al-Sheikh M, Sadda SR. Choriocapillaris Imaging Using Multiple En Face Optical Coherence Tomography Angiography Image Averaging. *JAMA Ophthalmol*. 2017;135(11):1197-1204. doi:10.1001/jamaophthalmol.2017.3904

17. Uji A, Balasubramanian S, Lei J, Baghdasaryan E, Al-Sheikh M, Sadda SR. Impact of Multiple En Face Image Averaging on Quantitative Assessment from Optical Coherence Tomography Angiography Images. *Ophthalmology*. March 2017. doi:10.1016/j.ophtha.2017.02.006

18. Zhang Q, Zheng F, Motulsky EH, et al. A Novel Strategy for Quantifying Choriocapillaris Flow Voids Using Swept-Source OCT Angiography. *Invest Ophthalmol Vis Sci*. 2018;59(1):203-211. doi:10.1167/iovs.17-22953

19. Borrelli E, Uji A, Sarraf D, Sadda SR. Alterations in the Choriocapillaris in Intermediate Age-Related Macular Degeneration. *Invest Ophthalmol Vis Sci*. 2017;58(11):4792-4798. doi:10.1167/iovs.17-22360

20. Spaide RF. Choriocapillaris Flow Features Follow a Power Law Distribution: Implications for Characterization and Mechanisms of Disease Progression. *Am J Ophthalmol*. 2016;170:58-67. doi:10.1016/j.ajo.2016.07.023

21. Spaide RF, Fujimoto JG, Waheed NK. IMAGE ARTIFACTS IN OPTICAL COHERENCE TOMOGRAPHY ANGIOGRAPHY. *Retina Phila Pa*. 2015;35(11):2163-2180. doi:10.1097/IAE.0000000000000765

22. Zhang Q, Zhang A, Lee CS, et al. Projection artifact removal improves visualization and quantitation of macular neovascularization imaged by optical coherence tomography angiography. *Ophthalmol Retina*. 2017;1(2):124-136. doi:10.1016/j.oret.2016.08.005

23. Uji A, Balasubramanian S, Lei J, Baghdasaryan E, Al-Sheikh M, Sadda SR. Choriocapillaris Imaging Using Multiple En Face Optical Coherence Tomography Angiography Image Averaging. *JAMA Ophthalmol*. October 2017. doi:10.1001/jamaophthalmol.2017.3904

24. Schneider CA, Rasband WS, Eliceiri KW. NIH Image to ImageJ: 25 years of image analysis. *Nat Methods*. 2012;9(7):671-675.

25. Spaide RF. CHORIOCAPILLARIS SIGNAL VOIDS IN MATERNALLY INHERITED DIABETES AND DEAFNESS AND IN PSEUDOXANTHOMA ELASTICUM. *Retina*. January 2017:1. doi:10.1097/IAE.0000000000001497

26. Yehoshua Z, Garcia Filho CAA, Penha FM, et al. Comparison of geographic atrophy measurements from the OCT fundus image and the sub-RPE slab image. *Ophthalmic Surg Lasers Imaging Retina*. 2013;44(2):127-132. doi:10.3928/23258160-20130313-05

27. Bearelly S, Chau FY, Koreishi A, Stinnett SS, Izatt JA, Toth CA. Spectral domain optical coherence tomography imaging of geographic atrophy margins. *Ophthalmology*. 2009;116(9):1762-1769. doi:10.1016/j.ophtha.2009.04.015

28. Drexler W, Sattmann H, Hermann B, et al. Enhanced visualization of macular pathology with the use of ultrahigh-resolution optical coherence tomography. *Arch Ophthalmol Chic Ill 1960*. 2003;121(5):695-706. doi:10.1001/archopht.121.5.695

29. Borrelli E, Souied EH, Freund KB, et al. REDUCED CHORIOCAPILLARIS FLOW IN EYES WITH TYPE 3 NEOVASCULARIZATION AND AGE-RELATED MACULAR DEGENERATION. *Retina Phila Pa*. April 2018. doi:10.1097/IAE.0000000000002198

30. Matet A, Daruich A, Hardy S, Behar-Cohen F. PATTERNS OF CHORIOCAPILLARIS FLOW SIGNAL VOIDS IN CENTRAL SEROUS CHORIORETINOPATHY: An Optical Coherence Tomography Angiography Study. *Retina Phila Pa*. July 2018. doi:10.1097/IAE.0000000000002271

31. Ahn J, Yoo G, Kim JT, Kim S-W, Oh J. Choriocapillaris layer imaging with swept-source optical coherence tomography angiography in lamellar and full-thickness macular hole. *Graefes Arch Clin Exp Ophthalmol Albrecht Von Graefes Arch Klin Exp Ophthalmol*. 2018;256(1):11-21. doi:10.1007/s00417-017-3814-7

32. Dodo Y, Suzuma K, Ishihara K, et al. Clinical relevance of reduced decorrelation signals in the diabetic inner choroid on optical coherence tomography angiography. *Sci Rep*. 2017;7(1):5227. doi:10.1038/s41598-017-05663-9

33. Nassisi M, Lavia C, Alovisi C, Musso L, Eandi CM. Short-Term Choriocapillaris Changes in Patients with Central Serous Chorioretinopathy after Half-Dose Photodynamic Therapy. *Int J Mol Sci*. 2017;18(11). doi:10.3390/ijms18112468

34. Takahashi A, Ooto S, Yamashiro K, et al. Pachychoroid Geographic Atrophy: Clinical and Genetic Characteristics. *Ophthalmol Retina*. 2018;2(4):295-305. doi:10.1016/j.oret.2017.08.016

35. Lujan BJ, Rosenfeld PJ, Gregori G, et al. Spectral domain optical coherence tomographic imaging of geographic atrophy. *Ophthalmic Surg Lasers Imaging Off J Int Soc Imaging Eye*. 2009;40(2):96-101.

36. Hariri A, Nittala MG, Sadda SR, Strauss EC, Lai P, Henry E. Outer Retinal Tubulation as a Predictor of the Growth Rate of Geographic Atrophy in Age-related Macular Degeneration. *Invest Ophthalmol Vis Sci*. 2014;55(13):5885-5885.

37. Schaal KB, Gregori G, Rosenfeld PJ. En Face Optical Coherence Tomography Imaging for the Detection of Nascent Geographic Atrophy. *Am J Ophthalmol*. 2017;174:145-154. doi:10.1016/j.ajo.2016.11.002

38. Yehoshua Z, de Amorim Garcia Filho CA, Nunes RP, et al. Comparison of Geographic Atrophy Growth Rates Using Different Imaging Modalities in the COMPLETE Study. *Ophthalmic Surg Lasers Imaging Retina*. 2015;46(4):413-422. doi:10.3928/23258160-20150422-03

39. Yehoshua Z, Rosenfeld PJ, Gregori G, et al. Progression of geographic atrophy in age-related macular degeneration imaged with spectral domain optical coherence tomography. *Ophthalmology*. 2011;118(4):679-686. doi:10.1016/j.ophtha.2010.08.018

Figure Legends

Figure 1. Images derived from two different acquisitions (A and B) underwent an identical post-acquisition quality enhancement strategy by signal compensation and averaging, in order to obtain the final high quality image of the choriocapillaris flow (C). For each acquisition a 10 µm thick slab between 31 and 41 µm under the RPE reference was segmented to extract an *en-face* image of the choriocapillaris from the angiogram (D) and the structural OCT (E). After being inverted and blurred (G), the structure image was multiplied with the angiogram (D) in order to compensate the angiogram for regions of signal loss (e.g. under drusen). The resultant compensated angiogram images (F) were then registered and averaged to obtain the final Choriocapillaris *en-face* angiogram (C).

Figure 2. The OCT fundus image (A) was used for the manual delineation of the geographic atrophy (GA) area. The compensated, averaged choriocapillaris angiogram (B) was binarized and analyzed for percentage of flow voids in two concentric 500 µm wide areas around the GA (C and D). The inner ring was defined as the *para-atrophy zone* (C), while the outer ring was defined as the *peri-atrophy zone* (D).

Figure 3. The OCT fundus image (A) was used for the manual delineation of the geographic atrophy (GA) area while the averaged angiogram of the superficial vascular complex (B) was used as a reference to identify the foveal center. In the compensated, averaged choriocapillaris angiogram (C) a 500x500 µm square area (#) was drawn at the innermost point of the outer boundary of the *para-atrophy zone;* all possible positions for drawing a similar square equidistant from the fovea were considered within the *peri-atrophy zone* (*)*. Among these positions, the square which was most similar in distance to the foveal center as the peri-foveal square was selected for comparative analysis (D).
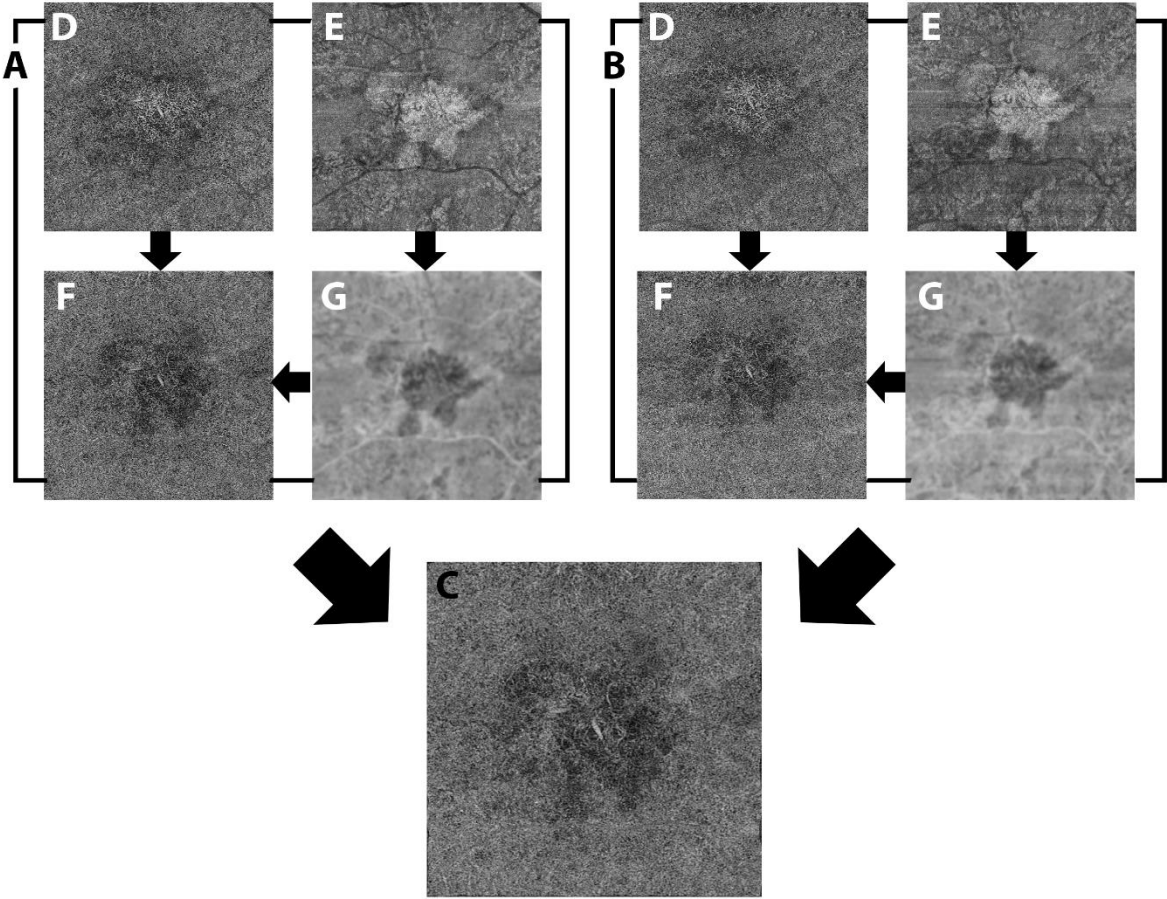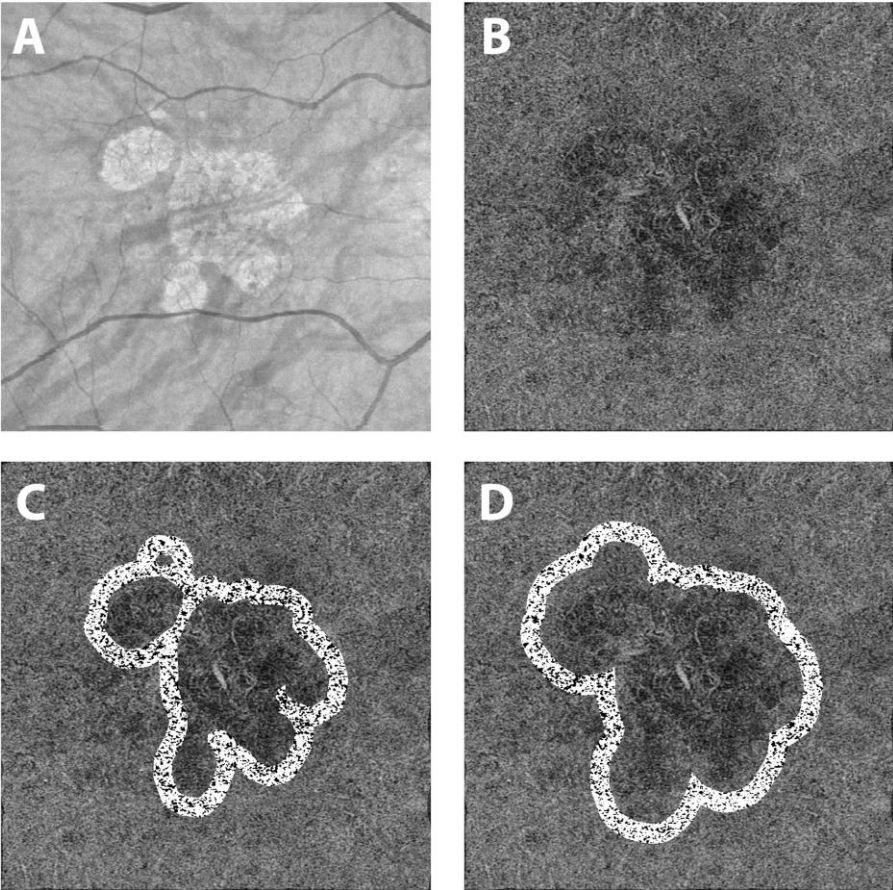
Figure 1

Figure 2

Figure 3